Interfaces at internal chills in solidifying steel sections

IOP Conf. Series: Materials Science and Engineering **529** (2019) 012054 doi:10.1088/1757-899X/529/1/012054

Interfaces at internal chills in solidifying steel sections

Charles Monroe[1], Robin Foley[1], John Griffin[1], Sean Gibbons[2], Alec Saville[3]

[1]University of Alabama at Birmingham, Birmingham, AL 35294-4461, USA
[2]Air Force Research Laboratories, Munitions Directorate, Eglin AFB
[3]Colorado School of Mines

camonroe@uab.edu

Abstract. Chills are used in the production of metal castings as a thermal aid to promote directional solidification in casted sections. This study will review microstructure and thermal circumstances of the internal chill interface where the chill is intended to be incorporated into the structure of the cast section. The conditions for interface coherency of cast steel sections from 25 to 50mm will be shown. Solidification proceeds away from the interface chill growing to a maximum thickness and then melting back to the original chill geometry. Furthermore, it is shown that promoting section solidification prior to the complete melting of the internal chill can lead to the formation of interfaces will be coherent across the chill and cast sections for compatible steel alloys. A computer model of the heat transfer and interface evolution show the possibility of using the coherent interface of internal chills in the design of other cast components.

1. Background

In the heating of materials, there are many methods and sources to add energy. During cooling, the number of methods and sources to accelerate heat extraction are more limited. Chills represent one of these few methods to enhance the cooling process. The enhancement in cooling using a chill is relative to the increase in conductivity and heat capacity of the chill material. Chills are standard manufacturing processing aids utilized within the metal casting industry [1]. The intent of the chill is to promote directional solidification which improves material soundness and properties. In some mining and wear applications, internal chills have been used in various methods of creating bimetallic, cast bonded, or hard-faced components [2-6]. This process takes the existing solid section (i.e., the internal chill) and through thermal bonding with the solidifying cast material creates one coherent monolithic structure, with components capable of exhibiting properties of both materials. In all of the cases, cooling rate of liquid metals during solidification and the respective configuration play a key role in the resulting interfacial reaction, but to this point only limited work has been completed to computational represent the reaction and to predict the coherency of the interface when using a chill in a cast solidification process.

Process modeling of metal casting is common in industry to understand solidification sequence and design the gating system for cast sections. Using computational fluid dynamics (CFD) to calculate the fluid flow and heat transfer is essential to the final results studied using MAGMAsoft [7]. However, assumptions typical to this process are limited to standard process conditions. A typical process models does not allow the melting of the chill and therefore conditions for a coherent interface are not predicted. To better understand the evolution of solidification at the interface of internal chills, two models for the interface of an internal chill are shown. First an analytical solution for a chill interface is proposed and

used to show the governing parameters and second an axisymmetric one-dimensional enthalpy method for solving the energy balance is used and implemented in MATLAB [8].

2. Method

To motivate the stability of the interface at an internal chill interface, an analytical solution of interface velocity including material properties and initial temperatures is shown. This method was developed in the book by Dantzig and Tucker and is reproduced here for completeness [9]. The internal chill for this example is calculated as one-dimensional solution in an infinite medium. The material used in this example is assumed to be a pure material with a single melting temperature with no diffusion. The first region of the internal chill, second region of solid growth, and third region of superheated liquid have equations for energy and initial/boundary conditions that are shown as,

$$\frac{\partial u}{\partial t} = \alpha_k \frac{\partial^2 u}{\partial x^2}, \tag{1a}$$

$$u = u_0(x \to -\infty), u = u_s(x = 0), u = u_m\big(x = \delta(t)\big), u = u_\infty(x \to \infty), \tag{1b}$$

where u, x, and t are the temperature, distance, and time respectively and α is the thermal diffusivity with subscript k substituting for the internal chill with i, solid growing away from chill with s, and superheated liquid with l. The initial/boundary conditions are shown for the internal chill as u_0 with increasing temperature the surface temperature u_s, the melt temperature is u_m, and the superheat temperature is u_∞. The solution for the three regions, chill, solid, and liquid are

$$u = u_s + (u_0 - u_s) erf\left(\frac{-x}{2\sqrt{\alpha_i t}}\right), -\infty < x \le 0. \tag{2a}$$

$$u = u_s + \frac{(u_m - u_s)}{erf(\phi)} erf\left(\frac{x}{2\sqrt{\alpha_s t}}\right), 0 \le x \le \delta(t) \tag{2b}$$

$$u = u_\infty + \frac{(u_m - u_\infty)}{erf\left(\phi\sqrt{\frac{\alpha_s}{\alpha_l}}\right) - 1}\left[erf\left(\frac{-x}{2\sqrt{\alpha_l t}}\right) - 1\right], \delta(t) \le x < \infty \tag{2c}$$

where $\delta(t)$ is the distance of the growth of this solid/liquid interface which changes as a function of time. The region of solid growth grows assuming a constant surface temperature determining both position of the interface and temperature of the surface equated the fluxes at x equals zero shown as

$$\delta(t) = 2\phi\sqrt{\alpha_s t}, \text{ and } u_s = \frac{u_0\sqrt{k_i\rho_i c_{pi}} erf(\phi) + u_m\sqrt{k_s\rho_s c_{ps}}}{\sqrt{k_i\rho_i c_{pi}} erf(\phi) + \sqrt{k_s\rho_s c_{ps}}}, \tag{3}$$

where ϕ is a constant that will be found using the Stefan condition, k, ρ, and c_p are the thermal conductivity, density, and specific heat for materials. The combination of these properties has been termed the heat diffusivity in contrast to the thermal diffusivity. For the purpose of this discussion, these are considered different because of the average temperatures of these regions however from the assumptions of the internal chill and solid growth regions these materials are substantively the same. Using the Stefan condition at the location of the solid/liquid interface, the final transcendental equation which completes the analysis is found as

$$\frac{c_{ps}(u_m - u_0)}{L_f\sqrt{\pi}} = \left(\phi exp(\phi^2) + \frac{c_{ps}(u_m - u_\infty)}{L_f\sqrt{\pi}} \frac{exp\left[\left(1 - \frac{\alpha_s}{\alpha_l}\right)\phi^2\right]}{\left[erf\left(\phi\sqrt{\frac{\alpha_s}{\alpha_l}}\right) - 1\right]} \frac{\sqrt{k_l\rho_l c_{pl}}}{\sqrt{k_s\rho_s c_{ps}}}\right)\left(erf(\phi) + \frac{\sqrt{k_s\rho_s c_{ps}}}{\sqrt{k_i\rho_i c_{pi}}}\right). \tag{4}$$

To determine the stable interface condition, the solid growth constant must be zero or $\phi = 0$. Therefore, equation (4) reduces to the relationship

$$(u_m - u_0)\sqrt{k_i\rho_i c_{pi}} = (u_\infty - u_m)\sqrt{k_l\rho_l c_{pl}} \tag{5}$$

A quick survey of liquid and solid material properties will demonstrate that the ratio of the heat diffusivity of liquid and solid is less than one but still on the order of one. This results in a stationary interface condition when the initial temperature of the chill is closer to the melt temperature than when the superheat temperature is to the melt temperature. This condition is opposite of metal casting practice where the initial temperature of the chill can be two orders of magnitude less than the superheat temperature. This result also shows that the solid growth velocity is slowed by increasing superheat temperatures. Therefore, it is expected that the solid/liquid interface will grow with a rate between 0 and a maximum when the superheat is zero. The conclusion is that only in the case of significant chill preheat temperatures will an internal chill melt rather than grow solid from the chill interface. This fundamental result also gives some insight into a parameter for a coherent interface, surface undercooling or $u_m - u_s$. At a stationary interface the solution of the surface undercooling is zero and the surface temperature is the same as the melt temperature. At all positive interface velocities, the undercooling increases and can be significant as

$$u_m - u_s = (u_m - u_0)\left(1 + \frac{\sqrt{k_s \rho_s c_{ps}}}{\sqrt{k_i \rho_i c_{pi}} erf(\phi)}\right)^{-1}. \quad (6)$$

The surface undercooling will vary from zero when the interface is stable to a maximum approximately half of the temperature difference between the melt temperature and the initial chill temperature. From this result, the use of an internal chill will initially form solid until/unless the chill soaks with heat raising the far field temperature resulting in a reversal in the solidification. After this point the progression of solidification will reverse and melting toward the chill will begin. It is this sequence of events that is of interest in this work to develop conditions for nucleation and grow away from chill as well as melting and coherence across this interface.

Given the analysis above, it was decided to analyze a similar condition using the one-dimensional axisymmetric model implemented within MATLAB is evaluated using the PDEPE command. The material properties in this domain can be calculated for the chill and matrix material using calculation of phase diagram or CALPHAD approaches with respect to the measured composition [10]. A mesh with uniform 100 elements across the chill dimension, uniform 100 elements across the cast dimension, and logarithmic spaced 40 across the mold dimension and result is shown in Figure 1. A typical result of temperature as a function of time and space from this model is shown with the heating of the chill near the axis of symmetry, solidification in the cast region, and heating in the mold according to the initial temperature. This result can be expressed in the chill and cast materials as a function of solid fraction shown with a similar angle as the temperature field as well as a contour plot with regions identifying the chill and cast materials. This result shows that the solid fraction initially grows from the chill interface but eventually the solidification front arrests reversing direction and melting toward the chill. This melting front continues until the outside solidification front freezes the entire structure.

This approach is a continuum solution which assumes a fixed thermodynamic path for the heating, cooling, and solidification. The materials for the matrix and for the internal chill material are summarized in Table 1 below. The chill material, 4330V, alloy targets include significant nickel, chromium, and molybdenum content [11]. These elements are absent from the matrix materials of WCB [12] with a maximum carbon target of 0.3 weight percent which will result in a material with similar or lower carbon than the 4330V chill and thus a higher melting temperature.

Table 1. Compositions selected for material in hybrid experiment.

ID	C wt%	Si wt%	Mn wt%	Cr wt%	Mo wt%	Ni wt%	Cu wt%	V wt%	Pour °C
4330V	*0.32*	*0.25*	*0.9*	*0.8*	*0.45*	*1.8*	*0*	*0.08*	*30*
WCB	*0.228*	*0.481*	*0.955*	*0.042*	*0.01*	*0.0299*	*0.0552*	*0.0295*	*1620*

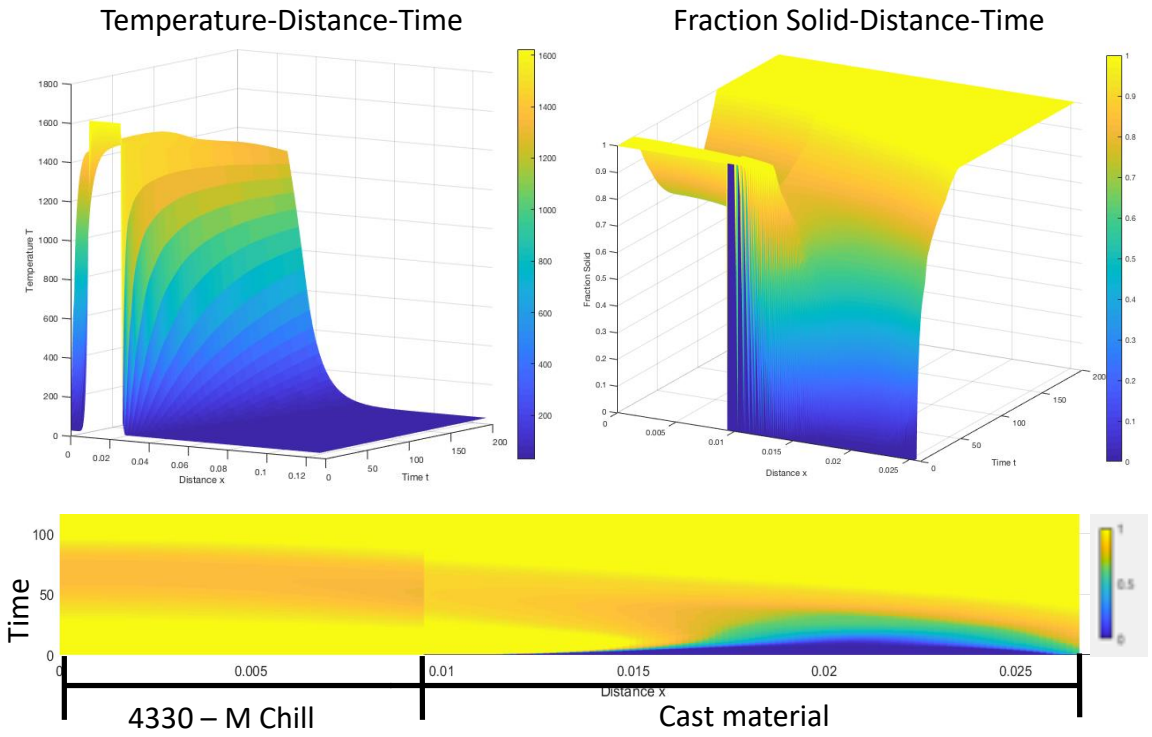

Figure 1. Example solution of energy equation for a chill, matrix, and mold domain is shown.

The geometry shown in Figure 2 illustrates the configuration of the chill and matrix material. The casting was manufactured using a sand mold bonded with a phenolic urethane binder system assembled with the internal chill rods. The rods were prepared prior to pouring using sand blasting. The melting was accomplished using an induction melting system with a liquid argon drip protective atmosphere. Alloys were prepared using low carbon steel feedstock material, ferromanganese, and ferrosilicon which was poured directly from the furnace. Target pouring temperature was ~100 degrees above the liquidus of the matrix material. The pour time was approximately 9 seconds. After shakeout, the gating system was removed, and the castings were sectioned at three heights as shown on Figure 2 labeled. To estimate the preheat temperature distribution in the MATLAB code the surface of the chill and the mold was held at the pour temperature for 0.1, 2, and 4 seconds respectively in the “A”, “B”, and “C” sections.

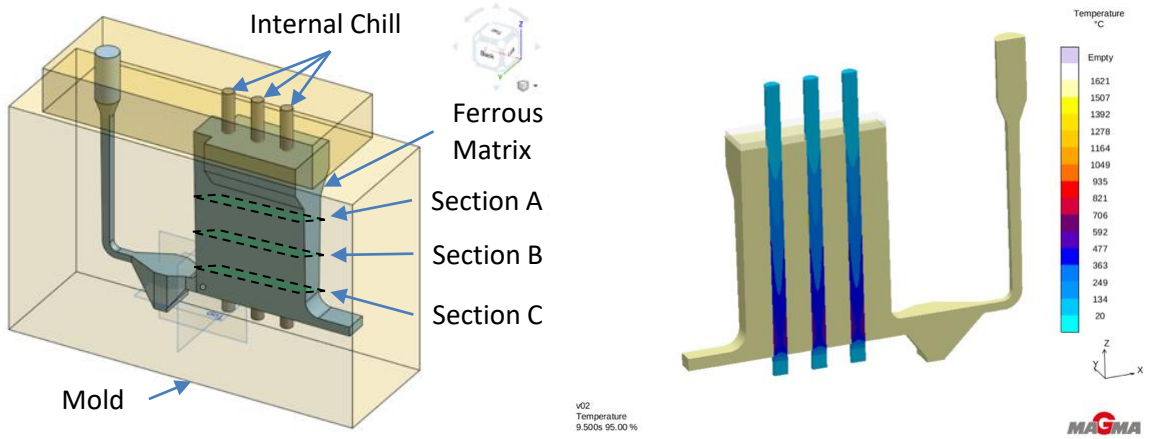

Figure 2. Geometry and mold setup used for the experimental process. Example temperature distribution at the midplane of the casting shown just after filling in 9 seconds.

3. Results

The commercial process simulation of the fluid flow shows significant heating during the filling process even after a short filling time of 9 seconds. Figure 2 shows an example of the temperature along the midplane of the casting just after filling with an estimate of temperature in the internal chill which exceeds 500 degrees Celsius. These results from the various combinations of size and temperature are compared to the experimental samples in Figure 3. All sections formed a coherent interface across the chill and matrix with a martensitic structure in the 4330V chill material and a pearlite structure in the WCB matrix. The microstructure is revealed using a nital etch. Figure 3 shows arrows the progression of solidification ending at the last to solidify area of the matrix. These solidification paths all follow the same progression of solid fraction shown and discussed for Figure 1. In the modeling result shown corresponds to the section size (A, B, or C) changed with the height. The initial temperature in the model was taken from the experimental value specified in Table 1 with one modification. The surface of the chill and mold was held at the pour temperature for 0.1, 2, and 4 seconds at sections A, B, or C respectively. In each case, the pattern of solidification away from the chill, arrest, and melting back was observed with resulting microstructures solidified from the outside to the interior. Due to the rapid heating at the thinnest section "C" during filling the microstructure had the slowest cooling rate and largest solidification features. In contrast, the shortest solidification time was near the top of the wedge in section "A", which showed evidence of fastest cooling rate and finer microstructural features. The center section "B" had mixed results with formation of a crack that extends through both the matrix and chill material. The orientation of the crack through the chill may confirm the coherence across the interface.

4. Conclusions

It appears that by controlling the flow, temperature, geometry, and composition of ferrous alloy that conditions for a coherent interface can be obtained. The key feature of the expected coherence of the interface appears to be the sequence of solidification determined by the surface undercooling. In the WCB and 4330 case, bonding was found at all locations and a significant chill layer and melting back of the chill layer was seen in the modeling. This mechanism looks like an important criterion to the prediction of bonding in ferrous/ferrous hybrid composites. Future work to couple the compositional effect as well as measurements of the microstructure demonstrating the cooling rate and other verification is ongoing.

References

[1] Ou, S., Carlson, K. D., Hardin, R., & Beckermann, C. (2002). Development of new feeding-distance rules using casting simulation: Part II. The new rules. *Metallurgical and Materials Transactions B*, *33*(5), 741–755.

[2] Lucey, T., Wuhrer, R., Moran, K., Reid, M., Huggett, P., & Cortie, M. (2012). Interfacial reactions in white iron/steel composites. *Journal of Materials Processing Technology*, *212*(11), 2349–2357.

[3] Qian, M., Harada, S., Yanxiang, L., & Dongjun, M. (1996). On the fabrication of steel-wire-reinforced white cast irons. *Materials Science and Engineering A*, *206*(1), 104–109.

[4] Wróbel, T. (2014). Characterization of Bimetallic Castings with an Austenitic Working Surface Layer and an Unalloyed Cast Steel Base. *Journal of Materials Engineering and Performance*, *23*(5), 1711–1717

[5] Cingi, C. (2010). Cast bonding of cast irons to ferritic stainless steels, *Materials Science Forum*

[6] Lucey, T., Wuhrer, R., Moran, K., Reid, M., Huggett, P., and Cortie, M., (2012). Interfacial reactions in white iron/steel composites, *Journal of Materials Processing Technology*, vol. 212(11), 2349–2357.

[7] MAGMA GmbH. *MAGMAsoft v5*, 52072 Aachen, Germany

[8] MATLAB Release 2017b, The MathWorks, Inc., Natick, Massachusetts, United States.

[9] Dantzig, J. A., & Tucker, C. L. (2001). Modeling in Materials Processing. Cambridge University

Press.
[10] Sente Software Ltd. *Jmatpro 9.0*, Surrey Research Park, United Kingdom
[11] ASTM A646 / A646M-17, Standard Specification for Premium Quality Alloy Steel Blooms and Billets for Aircraft and Aerospace Forgings, ASTM International, West Conshohocken, PA, 2017, www.astm.org
[12] ASTM A216 / A216M-18, Standard Specification for Steel Castings, Carbon, Suitable for Fusion Welding, for High-Temperature Service, ASTM International, West Conshohocken, PA, 2018, www.astm.org

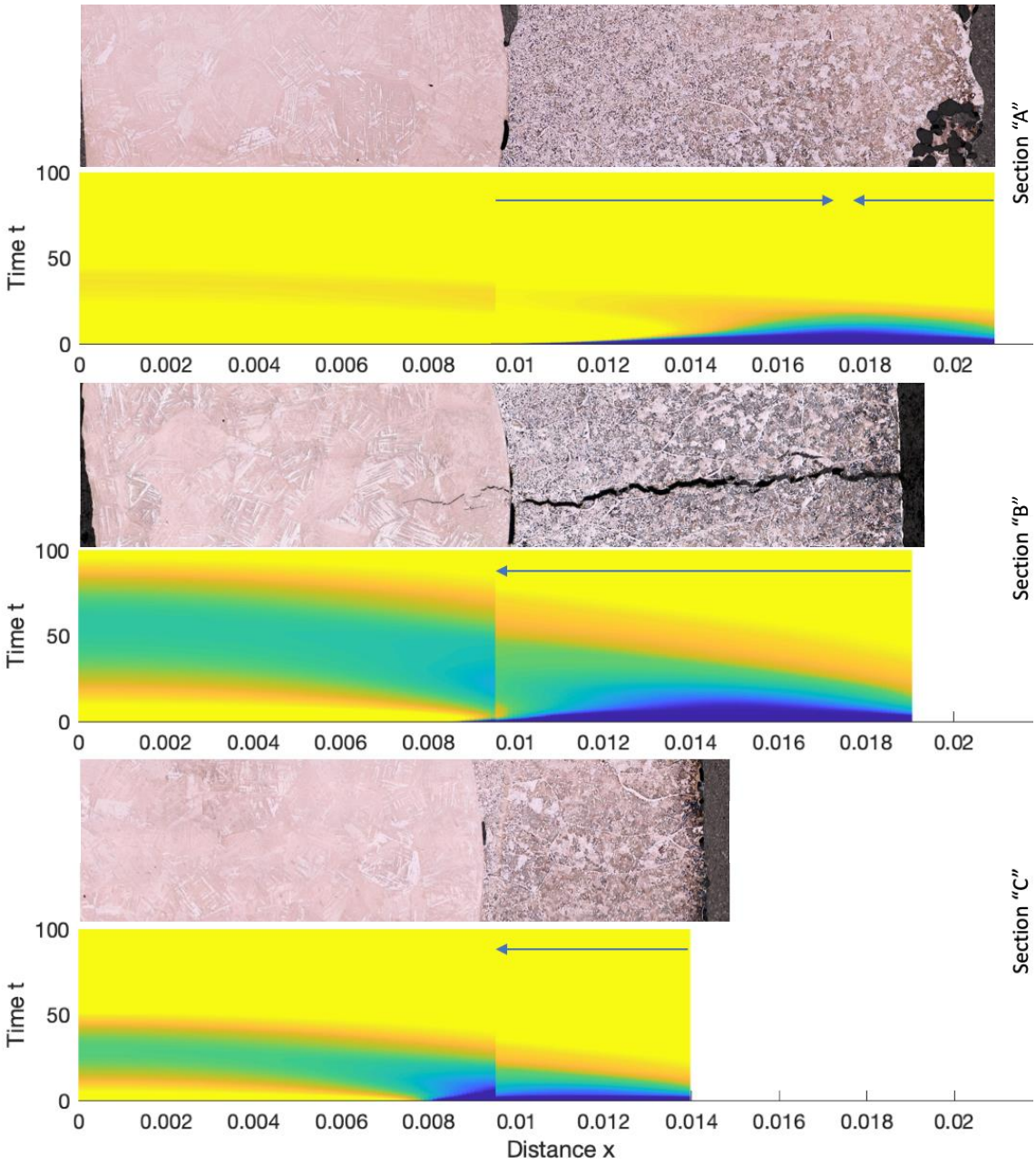

Figure 3. WCB and 4330 sections etched with nital compared to simulations, distance x in meters and time in seconds.